

Field measurement results of Tsing Ma suspension Bridge during Typhoon Victor

Y.L. Xu[†] and L.D. Zhu[‡]

Department of Civil and Structural Engineering, The Hong Kong Polytechnic University, Hung Hom, Kowloon, Hong Kong

K.Y. Wong^{‡†} and K.W.Y. Chan^{‡‡}

Tsing Ma Control Area Division, Highways Department, Hong Kong

Abstract. A Wind and Structural Health Monitoring System (WASHMS) has been installed in the Tsing Ma suspension Bridge in Hong Kong with one of the objectives being the verification of analytical processes used in wind-resistant design. On 2 August 1997, Typhoon Victor just crossed over the Bridge and the WASHMS timely recorded both wind and structural response. The measurement data are analysed in this paper to obtain the mean wind speed, mean wind direction, mean wind inclination, turbulence intensity, integral scale, gust factor, wind spectrum, and the acceleration response and natural frequency of the Bridge. It is found that some features of wind structure and bridge response are difficult to be considered in the currently used analytical process for predicting buffeting response of long suspension bridges, for the Bridge is surrounded by a complex topography and the wind direction of Typhoon Victor changes during its crossing. It seems to be necessary to improve the prediction model so that a reasonable comparison can be performed between the measurement and prediction for long suspension bridges in typhoon prone regions.

Key words: field measurement; Typhoon Victor; suspension bridge; wind characteristics; acceleration response; implication to buffeting analysis.

1. Introduction

With the increase of span length of modern suspension bridges, the prediction of bridge response to strong winds becomes more and more important for the bridge constructed within a wind-prone area. Some analytical methods, computational fluid dynamics technique, and wind tunnel test technique have been thus developed. To verify these analytical and numerical methods as well as wind tunnel tests, the filed measurements of wind characteristics and bridge response play an important role. To this end, wind and structural health monitoring systems have been installed in several long-span cable-supported bridges throughout the world to carry out field measurements. Among them is the

[†] Professor

[‡] Ph.D Candidate

^{‡†} Senior Engineer

^{‡‡} Engineer

one installed in the Tsing Ma suspension Bridge by the Highways Department of Hong Kong Special Administrative Region.

The Tsing Ma Bridge in Hong Kong is the longest suspension bridge in the world carrying a dual three-lane highway on the upper level of the bridge deck and two railway tracks and two carriageways on the lower level within the bridge deck (see Fig. 1). It is the key structure of the most important transportation network in Hong Kong that links the Hong Kong International Airport to the commercial centres of Hong Kong Island and Kowloon. The Tsing Ma Bridge is also located in one of the most active typhoon prone regions in the world. On 2 August 1997, about three months after the opening of the Tsing Ma Bridge, Typhoon Victor just crossed over the Bridge and made landfall over the western part of the New Territories. The WASHMS installed in the Bridge timely recorded wind speed and bridge response time-histories of seven hours duration (Lau *et al.* 1998).

This paper first describes Typhoon Victor, the Bridge and its surroundings, and the measurement instrumentation. The recorded wind and structural response data are then analysed to evaluate the mean wind speed, mean wind direction, mean wind inclination, turbulence intensity, integral scale, gust factor, wind spectrum, and the acceleration response and natural frequency of the Bridge. After a brief introduction of the currently used approach for predicting buffeting response of long suspension bridges, this paper finally utilises the measured results to highlight the importance of improvement of the currently used analytical process.

2. Typhoon Victor

Tropical depression Victor originated in the middle of the South China Sea on 31 July 1997 and its intensity continuously increased afterwards (Lee *et al.* 1998). The tropical depression Victor first moved north-westerly for 12 hours and then had a sudden turn to near north and remained in almost the same direction during its passage over Hong Kong (see Fig. 2). The tropical depression Victor became a real typhoon when it entered the region of 250 km south of Hong Kong at 8:00 on 2 August 1997 HKT (Hong Kong Time). At 19:00 HKT on 2 August, the centre of Typhoon Victor moved into the region about 8km east of Cheung Chau Island. The lowest air pressure measured on

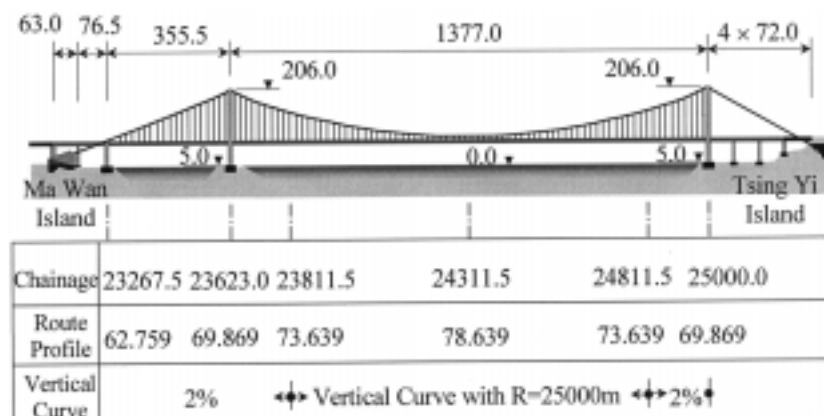


Fig. 1 Elevation of Tsing Ma Bridge

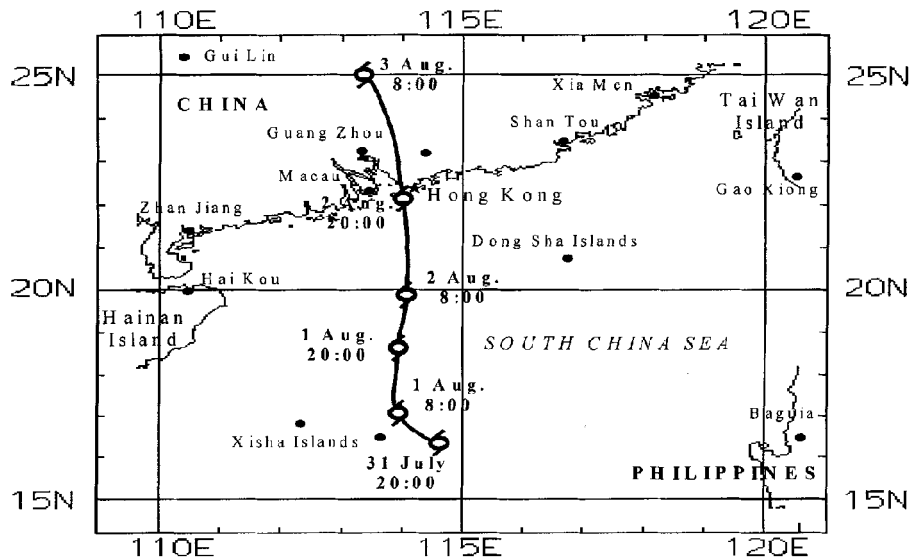


Fig. 2 Moving path of Typhoon Victor

Cheung Chau Island (see Fig. 3) at sea level was 972hPa. Typhoon Victor then crossed over the Tsing Ma Bridge at 20:05 and made landfall over the western part of the New Territories. Victor crossed over the whole Hong Kong within 2 hours at the average translational speed about 25km per hour. After leaving Hong Kong, Typhoon Victor continued moving in the north until it decayed on 3 August in the Southeast of China. The measured highest 10 minute mean wind speed in the wall area of the typhoon during its passage over Hong Kong was about 110 km per hour (30.6 m/s) at a 500 m height above the ground, just 2 hours after its landfall (Lee *et al.* 1998).

3. Tsing Ma Bridge and topography

The Tsing Ma Bridge has an overall length of 2160 m and a main span of 1377 m (see Fig. 1). The alignment of bridge deck deviates from the east-west axis for about 17° in anticlockwise (see Fig. 3). The bridge deck is 41 m wide and 7.63 m high. The two bridge towers of 206 m high are made of pre-stressed concrete. The east bridge tower sits on the Northwest shoreline of Tsing Yi Island, called the Tsing Yi Tower while the west bridge tower sits on Ma Wan Island, called the Ma Wan Tower.

Hong Kong is situated in the coastal area of South China. Not only there are many islands in Hong Kong, but also there are many mountains covering most areas of the territory (see Fig. 3). The local topography surrounding the Tsing Ma Bridge within the dashed circle of 5 km in radius includes sea, islands, and mountains of 69 to 500 m high. If taking the bridge as a centre, the surrounding area may be roughly classified into seven types of regions (I to VII), bounded by seven lines R1 (18° south of east), R2 (45° north of east), R3 (15° north of west), R4 (15° south of west), R5 (49° south of west), R6 (63° south of west), and R7 (40° east of south). Tsing Yi Island adjacent to the Bridge is in Region I and VII. The top levels of Tsing Yi Island are 218 m in the north (Region I) and 334 m in the south (Region VII). Ma Wan Island adjacent to the Bridge is in

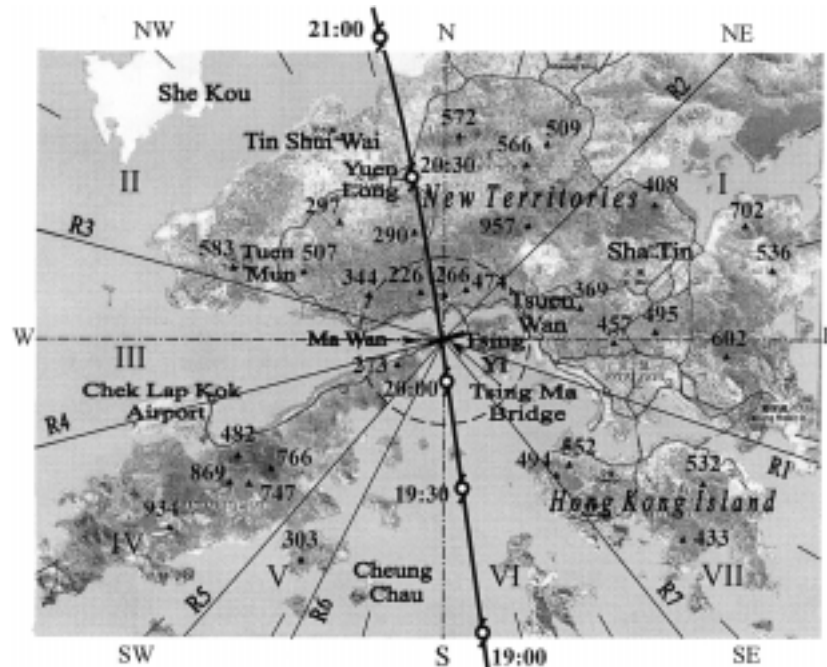


Fig. 3 Schematic diagram of the topography of Hong Kong

Regions III and IV. The top level of Ma Wan Island is 69 m only.

4. Instrumentation and data analysis

The WASHMS has seven different types of sensors: anemometer, temperature measurement assembly, accelerometer, strain gauge, level sensing system, displacement transducer, and weigh-in-motion systems (Lau *et al.* 1998). There are a total of six anemometers and 24 uni-axial servo type accelerometers installed in the Tsing Ma Bridge. Two digital Gill Wind Master ultrasonic anemometers (AneU) were installed on the north side and south side, respectively, of the bridge deck at the mid-span. They are specified as WITJN01 and WITJS01. Each ultrasonic anemometer can measure three components of wind velocity simultaneously. Two analogue mechanical anemometers (AneM) were located at two sides of the bridge deck near the middle of the Ma Wan side span, specified as WITBN01 at the north side and WITBS01 at the south side. Each analogue anemometer consists of a horizontal component (RM Young 05106) and a vertical component (RM Young 27106). Another two analogue mechanical anemometers (AneM) of horizontal component only were arranged at the level of 11 m above the top of each bridge tower on the south side. They are specified as WITPT01 for the Tsing Yi Tower and WITET01 for the Ma Wan Tower (see Fig. 4).

The servo accelerometers are of the brand Allied Signal Aerospace Q-Flex QA700. Three different types of arrangement for acceleration measurement were used in the system, namely AccT, AccB and AccU as indicated in Fig. 4, respectively representing Tri-axial measurement (three uni-axial accelerometers assembled orthogonally to each other), Bi-axial measurement (two uni-axial accelerometers assembled perpendicularly to each other) and Uni-axial measurement (by using only

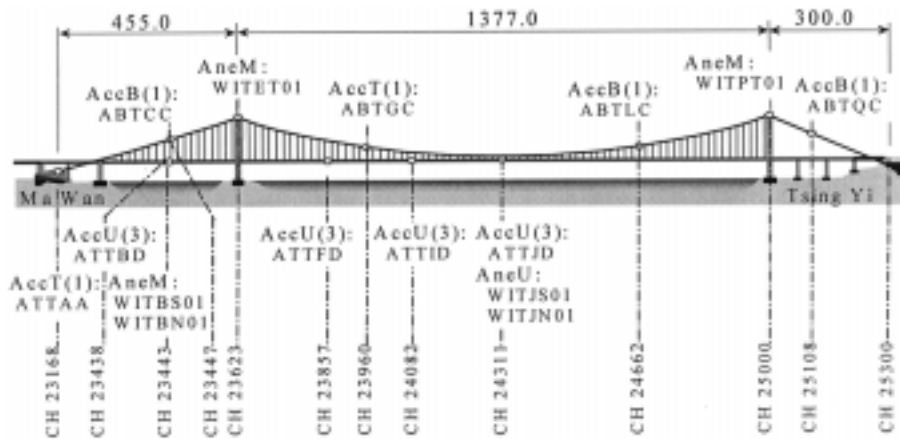


Fig. 4 Locations of anemometers and accelerometers

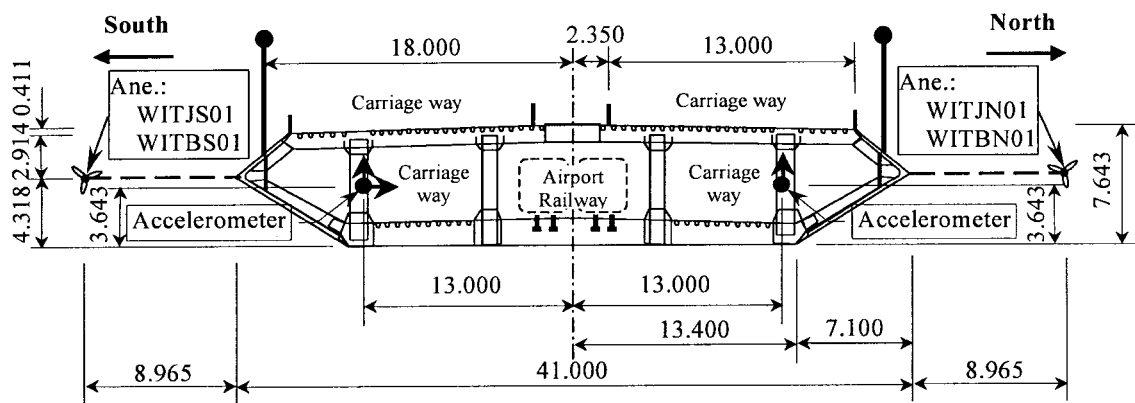


Fig. 5 Positions of sensors on cross section of bridge deck

one accelerometer to give signal in one prescribed direction). A total of 12 uni-axial accelerometers were located at the four sections of the bridge deck. At each section, there were two accelerometers measuring acceleration in the vertical direction and one accelerometer measuring acceleration in the lateral direction, as shown in Fig. 5. A set of three uni-axial accelerometers was located at Ma Wan Anchorage for seismic load measurement.

The wind speed and bridge response time-histories of seven hours duration from 17:00 to 24:00 HKT on 2 Aug 1997 recorded by the WASHMS were analysed. The sampling frequencies of measurement of wind speed and bridge acceleration response were set as 2.56Hz for recording wind speed and 25.6Hz for recording acceleration response, respectively. Thus, the data number of each time history is 64512 for wind speed and 645120 for bridge acceleration response. By using MATLAB as a platform, some programs were developed to analyse the measured data to obtain wind characteristics and bridge response. The frequency resolution is 0.00175Hz for the wind spectral analysis.

5. Wind structures

5.1. Mean wind

The 10-minute-averaged mean wind speed, mean wind direction, and mean wind inclination are presented first in this paper. Displayed in Figs. 6 and 7 are the variations of mean wind speed and mean wind direction, respectively, with time at the positions of the anemometers WITJS01, WITBS01, WITPT01, and WITET01. Fig. 7 shows that the mean wind to the Bridge blew from north-east in Region I between 17:00 and 19:50, and from south-west in Region V between 21:00 and 22:00, and from south-west in Region VI between 22:00 and 24:00. There was a sudden change of wind direction from north-east to south-west between 19:50 and 20:10. During this period, mean wind speed was very small as shown in Fig. 6. The reason for such a sudden change is that during this period, Typhoon Victor's eye just crossed over the Bridge. In consideration of the bridge alignment, the mean wind yaw angles between the mean wind direction measured at the top of the Tsing Yi Tower and the longitudinal axis of the Bridge were about 20° , 34° and 52° when the wind blew in Regions I, V, and VI, respectively.

The maximum 10-minute-averaged mean wind speeds were measured as 12.9 m/s at the deck level and 16 m/s at the tower-top level before Typhoon Victor crossed the Bridge. After the crossing, they became, respectively, 18.5 m/s and 21.1 m/s between 21:00 and 22:00, and 17.4 m/s and 23.3 m/s between 22:00 and 24:00. Clearly, the maximum 10-minute mean wind speed was larger after Typhoon Victor crossed the Bridge than before the crossing. For the horizontal distribution of mean wind speed, one may compare the mean wind speed measured from the anemometer WITJS01 with that from the anemometer WITBS01 (see Fig. 6) because they were arranged on the same side of the bridge deck with a horizontal distance about 860 m. Although the patterns of variation of the mean wind speed with time are similar to each other, there are some differences in the values of mean wind speed, particularly after the crossing of Typhoon Victor. The same feature can be also found in Fig. 8 for the mean speeds from the anemometers WITJN01 and WITBN01 which both are located on the north side of the bridge deck.

The mean wind speed profile during a typhoon is not well known yet. It also cannot be exactly explored this time, for only two level wind speeds are available. However, by fitting two level mean

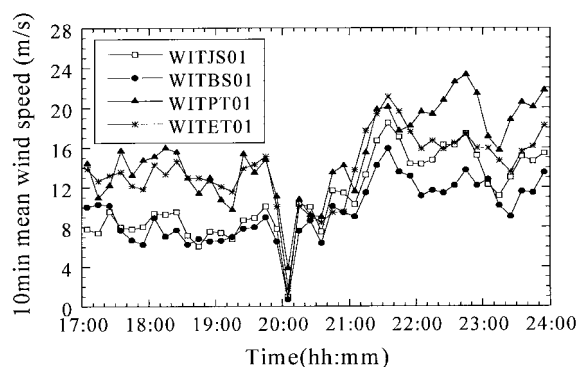


Fig. 6 Variation of 10 min mean wind speed (south side)

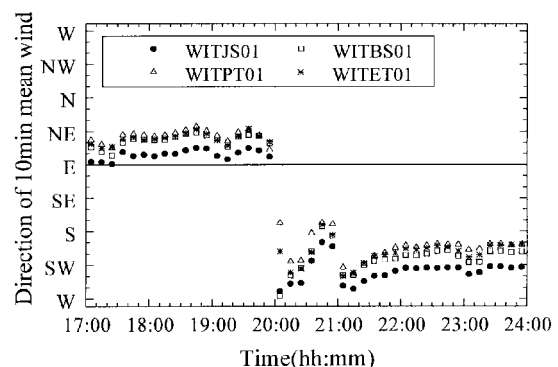


Fig. 7 Variation of 10 min mean wind direction (south side)

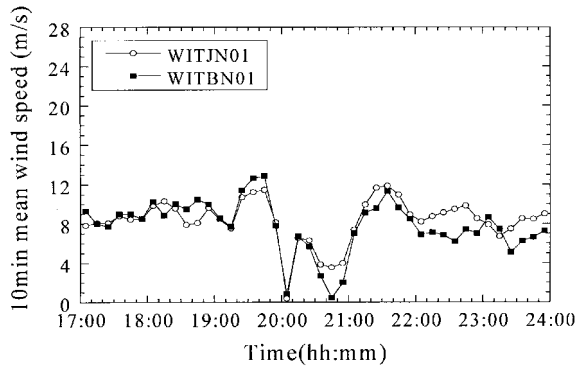


Fig. 8 Variation of 10 min mean wind speed (north side)

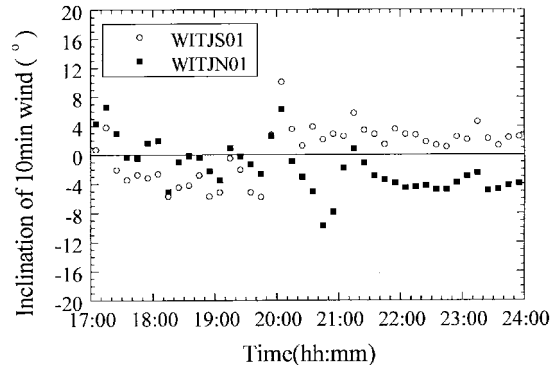


Fig. 9 Variation of 10 min mean wind inclination

wind speeds to the power law mean wind profile, it is found that the value of exponent for the power law varies with time. The mean value is about 0.324 when wind blew from north-east in Region I and 0.199 when wind blew from south-west in Region V.

The variation of mean wind inclination with time is shown in Fig. 9 for the anemometers near the mid-main-span of the Bridge (WITJS01 and WITBN01). It is seen that the mean wind inclination, that is, the angle between the mean wind direction and the horizontal plane, ranges from $+6^\circ$ to -6° . Occasionally, the wind inclination may reach $\pm 10^\circ$.

5.2. Turbulence intensity and integral scale

Turbulence intensity is the ratio of the standard deviation $\sigma(z)$ of the fluctuating wind to the mean wind speed $U(z)$ at the height z . It represents the intensity of the fluctuating wind and is expressed as

$$I_i = \frac{\sigma_i(z)}{U(z)} \quad i = u, v, w \quad (1)$$

where u , v , and w are the longitudinal, lateral, and vertical turbulence components, respectively. Figs. 10 and 11 display the longitudinal and lateral turbulence intensities at the top of the Ma Wan

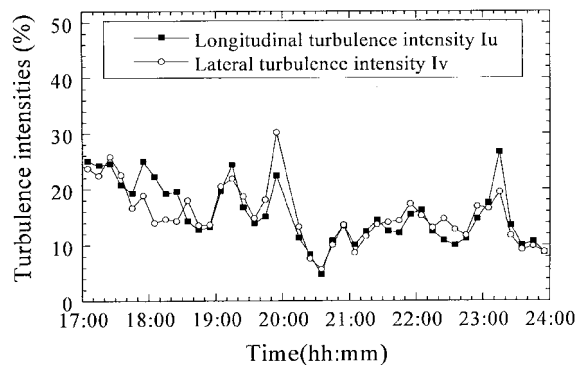


Fig. 10 Variation of turbulence intensity at WITET01

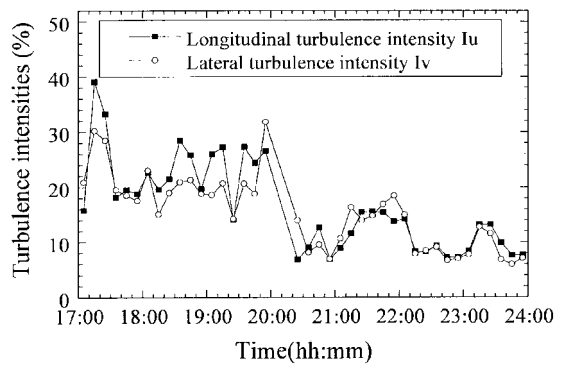


Fig. 11 Variation of turbulence intensity at WITPT01

Tower and the Tsing Yi Tower (206 m above the sea level), respectively, using the samples of 10 minutes duration. It is found that the mean longitudinal turbulence intensity at the top of the Ma Wan Tower (the anemometer WITET01) is 20.6% between 17:00 and 20:00 for Region I, 14.3% between 21:00 and 22:00 for Region V, and 14.0% between 22:00 and 24:00 for Region VI. Clearly, the longitudinal turbulence intensity varies with wind direction. The ratio of the mean lateral turbulence intensity to the mean longitudinal turbulence intensity at the top of the Ma Wan Tower is 0.97 for Region I, 1.05 for Region V, and 1.03 for Region VI. These ratios are much higher than those under the seasonal wind condition (Simiu and Scanlan, 1996). At the top of the Tsing Yi Tower (the anemometer WITPT01), the mean longitudinal turbulence intensity is 25.8% for Region I, 14.3% for Region V, and 10.0% for Region VI. Compared with those at the top of the Ma Wan Tower, one may find that turbulence intensity may not uniformly distribute along the longitudinal axis of the Bridge under the typhoon condition. Furthermore, the mean longitudinal turbulence intensity at the mid-main span of the deck is 30% for Region I, 15.8% for Region V, and 12.8% for Region VI. Compared with the same quantities at the top of the Ma Wan Tower and the Tsing Yi Tower, the mean longitudinal turbulence intensities at the deck level are larger at most time but occasionally smaller under the typhoon condition.

The integral scale of turbulence represents the average size of the turbulence eddies in the flow. The integral scales of the turbulence component u , v , and w in the mean wind direction can be estimated by

$$L_i^x = U \int_0^\infty C_i(\tau) d\tau \quad i=u, v, w \quad (2)$$

where $C_i(\tau)$ is the auto-variance function normalised by the variance. The mean integral scale of the turbulence component u at the top of the Tsing Yi Tower is 210 m between 17:00 and 20:00 for Region I, 243 m between 21:00 and 22:00 for Region V, and 294 m between 22:00 and 24:00 for Region VI. The ratio of the mean integral scale of the turbulence component v to the turbulence component u at the top of the Tsing Yi Tower is 0.54 for Region I, 0.78 for Region V, and 0.46 for Region VI, respectively. Clearly, these ratios obtained under the typhoon condition are much higher than those under the seasonal trade wind condition (Simiu and Scanlan 1996). It is also found that the mean integral scales at the top of the Tsing Yi Tower are different from those at the top of the Ma Wan Tower. The mean integral scales of the turbulence component u and w at the deck level are usually smaller than those at the top of the towers.

5.3. Gust factor

With respect to the gust factor based on the hourly mean wind speed, it is found that for a given longitudinal turbulence intensity, the factor is approximately proportional to the logarithm of gust duration (see Fig. 12). The factor is also almost proportional to longitudinal turbulence intensity for a given gust duration. Thus, by best fitting the measured data, the following empirical formula is obtained from the estimation of the gust factor during Typhoon Victor.

$$G(T, I_u) = 1 - 0.5377(I_u)^{1.082} \ln(T/3600) \quad (3)$$

where T is the gust duration in second and I_u is the longitudinal turbulence intensity.

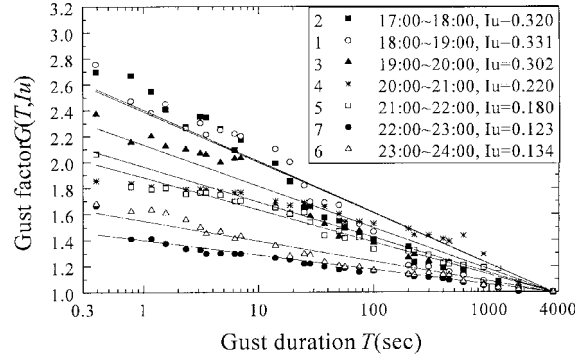


Fig. 12 Variation of gust factor with gust duration

5.4. Wind spectra

The auto-spectrum of turbulence describes wind energy distribution over frequency n . For the turbulence component u , von Karman (Morfiadakis *et al.* 1995), Kaimal *et al.* (1972) and Simiu and Scanlan (1996) presented Eq. (4), Eq. (5), and Eq. (6), respectively, as the normalised longitudinal auto-spectrum.

$$\frac{nS_u(n)}{u_*^2} = \frac{4\sigma_u^2 L_u^x n}{u_*^2 U [1 + 70.8(nL_u^x/U)^2]^{5/6}} \quad (4)$$

$$\frac{nS_u(n)}{u_*^2} = \frac{105f}{(1+33f)^{5/3}} \quad (5)$$

$$\frac{nS_u(n)}{u_*^2} = \frac{200f}{(1+50f)^{5/3}} \quad (6)$$

where $f=nz/U$. z is the height above the ground. Friction velocity u_* is estimated through the horizontal shear stress (Tieleman and Mullins 1980). The mean friction velocities are found to be 1.23, 1.09 and 0.86 m/s for Regions I, V and VI, respectively, at the deck level in this study.

For the turbulence component v , von Karman (Morfiadakis *et al.* 1995), Kaimal *et al.* (1972) and Simiu and Scanlan (1996) proposed Eq. (7), Eq. (8), and Eq. (9), respectively, as the normalised lateral auto-spectrum.

$$\frac{nS_v(n)}{u_*^2} = \frac{4\sigma_v^2 n L_v^x [1 + 755.2(nL_v^x/U)^2]}{u_*^2 U [1 + 283.2(nL_v^x/U)^2]^{11/6}} \quad (7)$$

$$\frac{nS_v(n)}{u_*^2} = \frac{17f}{(1+9.5f)^{5/3}} \quad (8)$$

$$\frac{nS_v(n)}{u_*^2} = \frac{15f}{(1+9.5f)^{5/3}} \quad (9)$$

For the turbulence component w , von Karman (Morfiadakis *et al.* 1995), Kaimal *et al.* (1972), and

Simiu and Scanlan (1996) recommended Eq. (10), Eq. (11), and Eq. (12), respectively, as the normalised vertical auto-spectrum.

$$\frac{nS_w(n)}{u_*^2} = \frac{4\sigma_w^2 nL_w^x [1 + 755.2(nL_w^x/U)^2]}{u_*^2 U [1 + 283.2(nL_w^x/U)^2]^{11/6}} \quad (10)$$

$$\frac{nS_w(n)}{u_*^2} = \frac{2f}{(1 + 5.3f)^{5/3}} \quad (11)$$

$$\frac{nS_w(n)}{u_*^2} = \frac{3.36f}{(1 + 10f)^{5/3}} \quad (12)$$

The spectral analysis is carried out in this study on the measured turbulence components at different locations and in different time periods using the samples of one-hour duration. The obtained auto-spectra are then compared with those expressed by Eqs. (4) to (12). It is found that the normalised auto-spectra of three components of fluctuating wind (nS_u/u_*^2 , nS_v/u_*^2 , nS_w/u_*^2) vary strongly with the time due to the change of wind direction and upwind terrain and also with the height of the anemometer position. It is also found that the von Karman spectra, using measured integral scales, fit the measured spectral much better than Kaimal and Simiu spectra, especially in the low frequency region. Figs. 13 to 15 display the longitudinal, lateral, and vertical wind spectra measured from WITJS01 during the period of 23:00 to 24:00 HKT.

The cross spectra between three turbulence components at each position are also analysed in this study. The cross-spectrum is a complex quantity. Its real part is called the co-spectrum, which is an even function of frequency n , and its imaginary part is named as the quadrature spectrum, which is an odd function of frequency n . The cross spectrum mainly describes the statistical dependence between the turbulence components at a given frequency n . A typical co-spectrum is plotted in Fig. 16 for the positive part only, which is measured from WITJS01 during the period of 23:00 to 24:00 HKT. The following empirical formulae of the co-spectrum suggested by Kaimal *et al.* (1972) is also plotted in Fig. 16 for positive part for a comparison.

$$\frac{nC_{uw}(n)}{u_*^2} = \frac{7f}{(1 + 9.6f)^{2.4}} \quad (13)$$

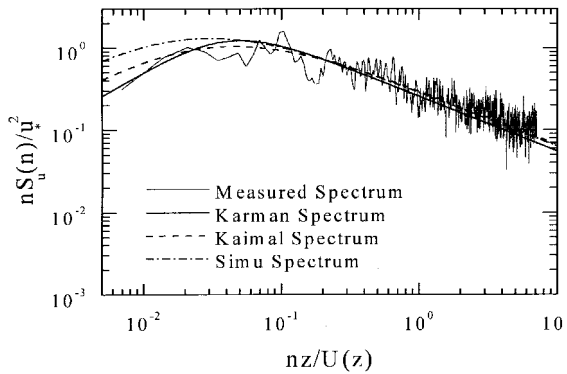


Fig. 13 Longitudinal spectrum at WITJS01

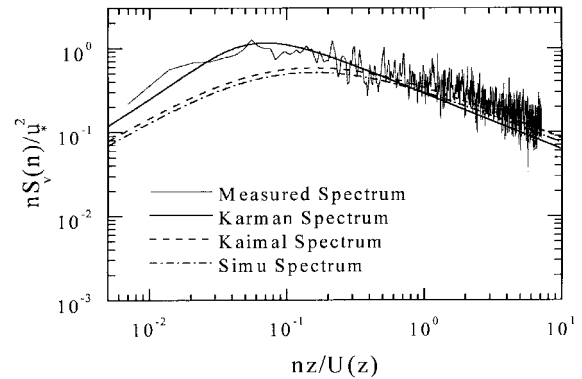


Fig. 14 Lateral spectrum at WITJS01

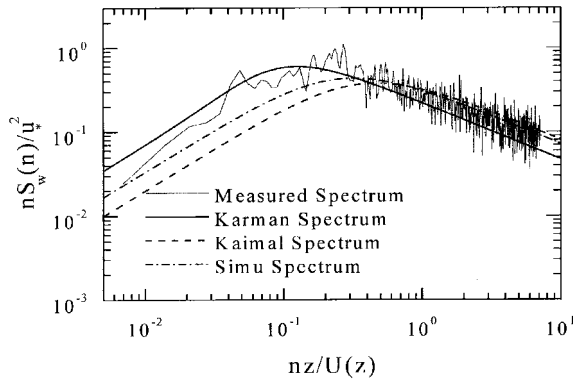


Fig. 15 Vertical spectrum at WITJS01

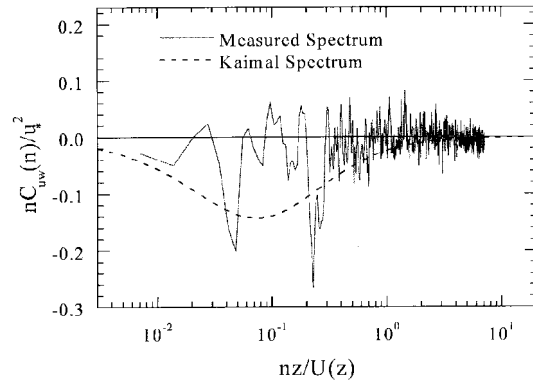


Fig. 16 Co-spectrum at WITJS01

6. Acceleration response

6.1. Bridge deck

Fig. 17 illustrates the time histories of lateral, vertical and torsional acceleration responses of the bridge deck at the mid-main span during the period of 18:00 to 24:00 HKT. The lateral response is directly taken from the lateral accelerometer. The vertical response is obtained by averaging the signals from the two vertical accelerometers. The torsional acceleration response is expressed as the difference between the two vertical signals and divided by 2. Fig. 18 shows the variations of standard deviations of lateral, vertical and torsional accelerations with time in 10-minute interval.

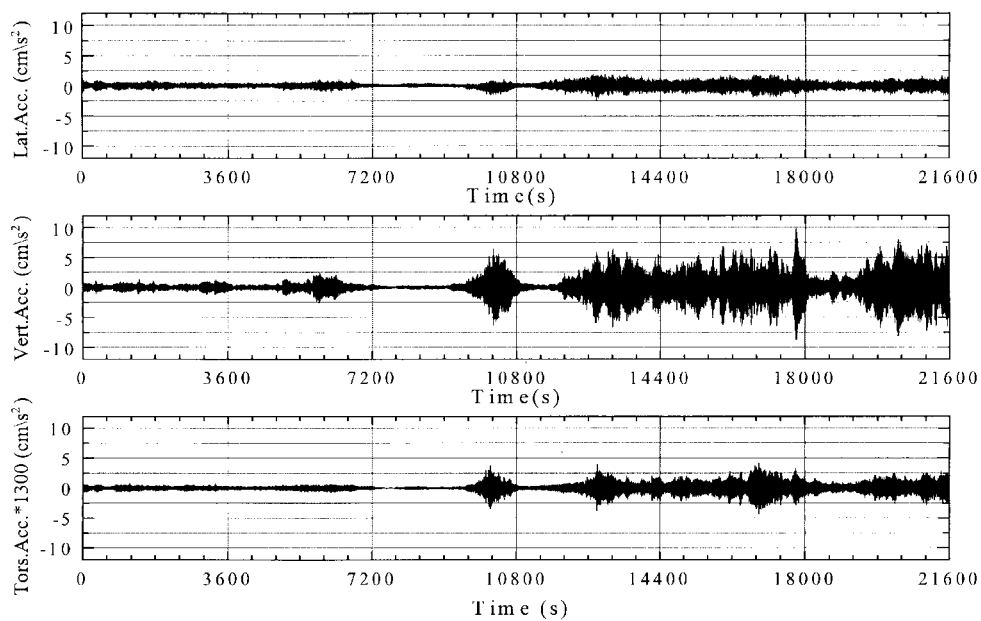


Fig. 17 Time histories of lateral, vertical and torsional accelerations

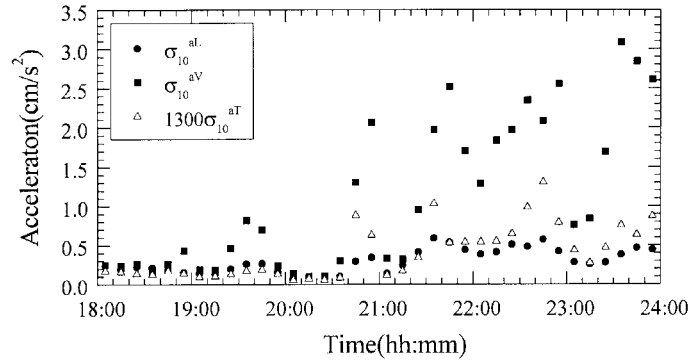


Fig. 18 Variation of standard deviation of acceleration response

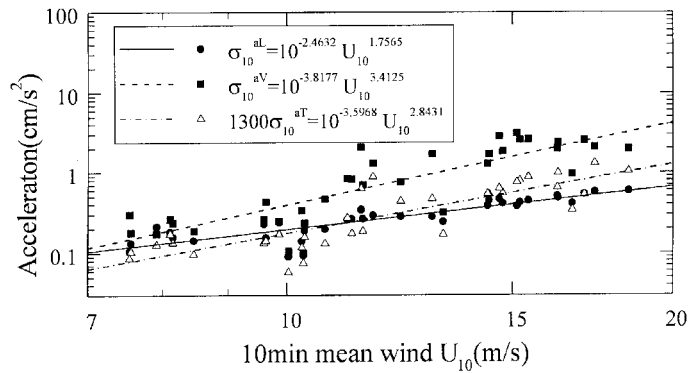


Fig. 19 Standard deviation acceleration response vs. mean wind speed

The maximum lateral, vertical and torsional standard deviation acceleration responses are found to be 0.588 cm/s^2 , 3.082 cm/s^2 and 0.0010 rad/s^2 , occurring at about 21:35, 23:35 and 22:45, respectively. Furthermore, by plotting the lateral, vertical, and torsional standard deviation acceleration responses against 10 minutes mean wind speed (see Fig. 19), it is seen that the vertical and torsional acceleration responses increase almost proportionally to the cube of mean wind speed. The lateral acceleration response increases almost proportionally to the square of mean wind speed. Clearly, the vertical acceleration is much larger than the lateral acceleration, and the vibration patterns are also different from each other.

6.2. Bridge cable

The acceleration responses of bridge cable at four positions are also analysed in this paper. The maximum lateral and vertical standard deviation acceleration responses of the main cable at the accelerometer ABTLC are 1.574 m/s^2 and 2.965 m/s^2 , occurring about 21:30 and 22:40, respectively. For the cable in the Tsing Yi side span, the maximum lateral and vertical standard deviation acceleration responses measured by the accelerometer ABTQC are 4.296 m/s^2 and 3.133 m/s^2 , respectively, at 23:50. Clearly, the lateral and vertical standard deviation acceleration responses of the bridge cable are sometime larger than those of the bridge deck.

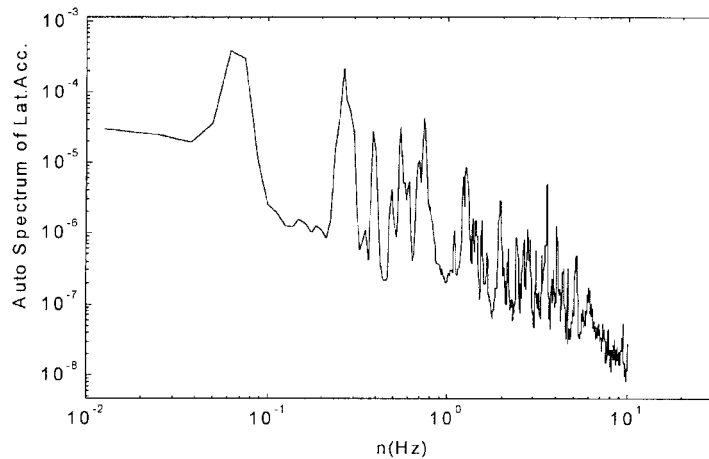


Fig. 20 Lateral acceleration spectra of the bridge at mid-span

6.3. Spectra and natural frequencies

The auto spectra of the lateral, vertical and torsional acceleration responses at the mid-span of the Bridge for the period of 22:00 to 23:00 were obtained from the response time histories. Fig. 20 shows only the auto spectrum of lateral acceleration response as an example. The first two peak frequencies identified from these spectra were 0.0688 Hz (0.068 Hz)[0.069 Hz] and 0.2656 Hz (0.285 Hz)[0.297 Hz] for lateral acceleration, and 0.2656 Hz (0.271 Hz)[0.267 Hz] and 0.4844 Hz (0.475 Hz) for torsional acceleration. The first three peak frequencies identified from the vertical spectrum were 0.1375 Hz (0.137 Hz) [0.139 Hz], 0.1813 Hz (0.189 Hz)[0.184 Hz] and 0.325 Hz (0.325 Hz)[0.327 Hz]. Compared with the numbers in the above parentheses and square brackets that were obtained by Xu *et al.* (1997) from the eigenvalue analysis and the ambient vibration measurement respectively, one can see that three sets of the natural frequency results are very close. The relative difference of the lateral frequencies is less than 11% and that of the torsional frequencies is less than 2% whilst that of the vertical frequencies is less than 4%. Furthermore, these frequencies were found to remain almost constant during the passage of Typhoon Victor in spite of the variation of the wind speed, wind direction, and upwind terrain.

7. Implications to analysis

The currently used buffeting analysis of long suspension bridges is mainly based on the Scanlans theory (Scanlan and Jones 1990, Jain *et al.* 1996). Such an analytical process is basically a combination of numerical, experimental, and analytical approaches. Finite element technique is usually used to determine the natural frequencies and mode shapes of a bridge. The wind tunnel tests of bridge section models provide flutter derivatives and aerodynamic coefficients. The buffeting response of bridge deck is then determined using the mode superposition method under the frame of random vibration theory. In general, it is assumed that mean wind is perpendicular to the bridge deck. The wind characteristics, such as mean wind speed, mean wind inclination, turbulence intensity, integral scale, and auto-spectrum, do not vary with the longitudinal axis of the

bridge. The wind forces on the bridge towers and cables are also not considered so that the wind-induced response of the bridge cables and towers and their interaction can not be predicted and estimated.

From the measured wind structures and bridge responses of the Tsing Ma Bridge during Typhoon Victor, it is clearly seen that for a long suspension bridge located in a complicated topography and attacked by a typhoon, wind direction may not be perpendicular to the longitudinal axis of the bridge. The mean wind speed, mean wind inclination, turbulence intensity, auto-spectrum, and others also vary with the longitudinal axis. The turbulence intensity and integral scale under the typhoon condition are usually higher than those used for the seasonal trade wind case. Thus, it will be difficult to have a reasonable comparison between the field measurement results and the prediction results. Furthermore, the responses of bridge cables are usually measured by a WASHMS. However, these results can not be used to facilitate the comparison. All these indicate the need of improvement of the currently used analytical process for predicting buffeting response of long suspension bridges in typhoon prone regions.

8. Conclusions

The wind and structural response data recorded by the Wind And Structural Health Monitoring System during Typhoon Victor were analysed in this paper for evaluating wind characteristics and acceleration response of the Tsing Ma suspension Bridge. The results show that during Typhoon Victor, both mean and turbulent characteristics varied considerably due to the change of wind direction and the complex upwind terrain. Turbulence intensities measured during Typhoon Victor were higher than those due to seasonal trade winds. The wind excitation mechanism of the Bridge in the lateral direction was different from that in the vertical direction or the rotation. The lateral and vertical acceleration responses of the bridge cable were sometime larger than those of the bridge deck. The implications of these measurement results to the currently used analytical process for predicting buffeting response of long suspension bridges were also given. It is necessary to have an improved analytical process for predicting the buffeting response of long suspension bridges in typhoon prone regions.

Acknowledgements

The work described in this paper was supported by both the Research Grants Council of Hong Kong through a grant to the first writer (Project No. PolyU 5027/98E) and the Hong Kong Polytechnic University through a studentship to the second writer. The support from the Tsing Ma Control Area Division, Highways Department of the Hong Kong, to allow the writers to access the measured data for academic purpose only is particularly appreciated. Any opinions and conclusions presented in this paper are entirely those of the writers.

References

Jain, A., Jones, N.P. and Scanlan, R.H. (1996), "Coupled flutter and buffeting analysis of long span bridges", *J.*

- of Struct. Engrg. ASCE*, **122**(7), 716-725.
- Kaimal, J.C., Wyngaard, J.C., Izumi, Y. and Cote, R. (1972), "Spectral characteristics of surface-layer turbulence", *J. Royal Meteorol. Soc.*, **98**, 132-148.
- Lau, C.K., Wong, K.Y. and Chan, K.W.Y. (1998), "Preliminary monitoring results of Tsing Ma Bridge", *The 14th National Conference on Bridge Engineering*, Shanghai, **2**, 730-740.
- Lee, P.W., Poon, H.T. and Lai, S.T. (1998), "Observational study of Typhoon Victor (9712) during its passage over Hong Kong", *12th Guangdong-HongKong-Macau Seminar on Hazardous Weather*, Hong Kong (in Chinese).
- Morfiadakis, E.E., Glinou, G.L. and Koulouvari, M.J. (1995), "The suitability of the von Karman spectrum for the structure of turbulence in a complex terrain wind farm", *J. Wind Eng. Ind. Aerodyn.*, **62**, 237-257
- Scanlan, R.H. and Jones, N.P. (1990), "Aeroelastic analysis of cable-stayed bridges", *J. of Struct. Engrg., ASCE*, **116**(2), 279-297.
- Simiu, E. and Scanlan, R.H. (1996), *Wind Effects on Structures*, John Wiley & Sons, INC, New York.
- Tieleman, H.W. and Mullins, S.E. (1980), "The structure of moderately strong winds at a Mid-Atlantic coastal site (below 75m)", *Proceedings of Fifth International Conference on Wind Engineering*, Pergamon Press, Oxford, **1**, 145-159.
- Xu, Y.L., Ko, J.M. and Zhang, W.S. (1997), "Vibration studies of Tsing Ma suspension Bridge", *J. Bridge Eng. ASCE*, **2**, 149-156.